Non-Stationary Rician Noise Estimation in Parallel MRI Using a Single Image: A Variance-Stabilizing Approach

Tomasz Pieciak, Santiago Aja-Fernández, and Gonzalo Vegas-Sánchez-Ferrero

Abstract—Parallel magnetic resonance imaging (pMRI) techniques have gained a great importance both in research and clinical communities recently since they considerably accelerate the image acquisition process. However, the image reconstruction algorithms needed to correct the subsampling artifacts affect the nature of noise, i.e., it becomes non-stationary. Some methods have been proposed in the literature dealing with the non-stationary noise in pMRI. However, their performance depends on information not usually available such as multiple acquisitions, receiver noise matrices, sensitivity coil profiles, reconstruction coefficients, or even biophysical models of the data. Besides, some methods show an undesirable granular pattern on the estimates as a side effect of local estimation. Finally, some methods make strong assumptions that just hold in the case of high signal-to-noise ratio (SNR), which limits their usability in real scenarios. We propose a new automatic noise estimation technique for non-stationary Rician noise that overcomes the aforementioned drawbacks. Its effectiveness is due to the derivation of a variance-stabilizing transformation designed to deal with any SNR. The method was compared to the main state-of-the-art methods in synthetic and real scenarios. Numerical results confirm the robustness of the method and its better performance for the whole range of SNRs.

Index Terms—MRI, parallel MRI, spatially variant noise, noise estimation, variance-stabilizing transformation, Rician distribution

1 Introduction

The Johnson-Nyquist (thermal) noise, coming from the stochastic motion of free electrons in a receiver coil, is one of the most dominant sources of deterioration in magnetic resonance imaging (MRI). Apart from the image quality impoverishment, this noise also affects further stages of the data processing pipeline, such as image segmentation or registration procedures [1], accuracy of tensor estimation in diffusion tensor imaging (DTI) [2], and fiber tracts reconstructions in diffusion tensor tractography [3], and fMRI analysis [4]. Moreover, noisy data might seriously affect the diagnostic performance of the image-derived metrics like signal-to-noise ratio (SNR) and contrast-to-noise ratio (CNR), or the evaluation of tumor tissues [5]. Consequently, an accurate modeling of the noise statistics is the keystone for better processing and interpretation of MRI data.

The noise distribution of magnitude MRI depends on the configuration of the acquisition system and the image reconstruction algorithm [6]. In single-coil systems, the noise component is assumed to be complex additive white Gaussian noise (AWGN) in the $\mathbf{k}-$space domain with constant variance over the whole field of view (FOV) [7]. This variance is proportional to the resistive impedance of the receiver coil and it is *pro rata* transposed to the spatial domain ($\mathbf{x}-$space) of the image by means of the inverse discrete Fourier transform (DFT). After the reconstruction process, the envelope (magnitude) of the complex signal follows a stationary Rician distribution [8], though in the background areas it reduces to a stationary Rayleigh due to the lack of water proton density.

Over the last decade, the use of phased array coil to acquire MRI data is systematically displacing single-coil devices. Multiple coil data requires an image reconstruction algorithm to combine the complex signals from each individual coil into a single composite image. Depending on the assumptions about the coil configuration and image model, different algorithms can be applied for this reconstruction, like those based on a spatial-matched-filter (SMF) [9] and on the sums of squares (SoS) [10]. In the first case, the image can be considered as non-stationary Rician, while in the second, it follows a noncentral chi (nc-χ) distribution [10]. However, if the correlation between coils is taken into account, the nc-χ assumption becomes just an approximation of the real distribution, and effective values must be considered [11].

If the acquisition is accelerated *via* a subsampling of the $\mathbf{k}-$space, the aliasing artifacts must be corrected using image reconstruction algorithms, known as parallel MRI (pMRI). Many different methods have been defined to reconstruct the final image from subsampled versions of the

signals in each coil, being SENSitivity Encoding (SENSE) [12] and GeneRalized Autocalibrating Partially Parallel Acquisition (GRAPPA) [13] dominant in commercial scanners. However, new reconstruction methods and modifications of the existing ones are continuously proposed. The use of these correction algorithms changes the underlying statistical model of the data. For SENSE imaging, the magnitude MRI signal is defined as non-stationary Rician [14] and for GRAPPA it can also be approximated by a non-stationary nc-χ distribution with an increased *effective variance of noise* and decreased *effective number of coils* [15].

Although numerous dedicated noise estimation schemes in MRI were proposed in the literature (an extensive review can be found in [16]), a substantial majority of them require multiple acquisitions, background identification or foreground extraction. Even in the case of automatic estimation based on a single image, like [16], [17], methods just estimate a single value for the variance of noise without considering its local variation, making them useless for spatially variant noisy patterns, such it is the case for modern acquisition systems.

Some computational techniques dealing with non-stationarity have been suggested in the literature. However, in most of the cases, their accuracy is limited due to the granularity caused by local estimation. Moreover, some of them require further information which is not always available in conventional *in vivo* examinations: receiver noise matrix [18], sensitivity coil profiles in SENSE and reconstruction coefficients for GRAPPA [19], biophysical model of the data [20] or repeated acquisitions [5], [20], [21], [22], [23].

In this paper, we propose an automatic method to estimate the spatially variant Rician noise from MR imaging. This kind of noise is particularly interesting since we can find it in SENSE acquisitions and in multiple coil reconstructions that use SMF. Compared to the state of the art, the proposed method shows the following advantages:

1) It does not depend on repeated acquisitions and/or a biophysical model of the data.
2) Any additional information like sensitivity profiles or noise matrices in the receiver coils are also unnecessary.
3) The noise map is estimated using only a single image without background or foreground region extraction.
4) It supports different contrast type examinations: T_1-weighted, T_2-weighted and PD-weighted MR data.
5) The method is not affected by granular effects due to local estimation.
6) The method is robust for the whole range of SNRs (from very low SNRs—non-stationary Rayleigh—to very high SNRs, non-stationary Gaussian noise).

The proposed method is developed by defining a suitable variance-stabilizing transformation (VST). This technique allows transforming the magnitude image from a non-stationary variate to a stationary variate. The proposed transformation provides a proper stabilization behavior throughout the whole range of SNRs and it is designed to provide Gaussian-like distributed variates. Afterward, the spatial variability of noise is retrieved by a homomorphic filtering. The proposal was compared to the most relevant state-of-the-art methods for non-stationary Rician noise estimation showing a remarkably better behavior.

2 Background

2.1 Non-Stationary Noise Estimation in MRI

Traditionally, noise estimators proposed in the literature determine a single value of σ for the whole image (e.g., [16], [44]). However, an increasing number of methods attempt to estimate non-homogeneous maps of noise in several fields related to imaging not strictly confined to the MRI context.

One of the first attempts for spatially variable noise estimation in Rician distributed data was proposed by Marzetta [24] and adapted by DeVore et al. [25] in the context of single-polarization synthetic aperture radar (SAR) images. Authors propose an expectation-maximization (EM) iterative algorithm to find maximum likelihood (ML) estimates of the parameters of a Rician distribution. To that end, multiple samples of the receiving signal are necessary.

In a more general context, Goossens et al. proposed in [26] a method to estimate the spatially variant map of noise in images assuming they are corrupted by a non-stationary AWGN process. The wavelet transform was used to separate the signal and the noise assuming that the high-high subband is strictly noise.

In the MRI field, the pioneers of spatially variable noise estimation were Samsonov and Johnson [18], defining a method to calculate the noise map from the receiver coil noise matrix, which, in fact, is not always available in a clinical routine. Delakis et al. [27] proposed a method to estimate spatially variant noise by suppressing the signal component without the need of extra information. To that end, they removed the low-low subband coefficients of the stationary wavelet transform (SWT) of the magnitude image. The estimation is done assuming that the signal component has been completely removed and the resulting image is Rayleigh distributed noise.

An alternative technique was proposed by Landman et al. [20], [28], based on a robust scale estimator followed by a regularization procedure using a coil sensitivity model. Although this method was proposed to cope with multiple independent MR scans, in its basic scenario it can be used to estimate the noise map from a single image.

Other significant estimation methods are the following: Guo and Huang [29] proposed a local variance as a noise level estimator after edges exclusion by means of local mutual information and k-means segmentation; Aja-Fernández et al. in [35] proposed a noise estimation approach for non-accelerated SoS reconstructed MR images from correlated multiple-coil; Maggioni and Foi [33] exploited the sparsity of the representation of similar 2D patches in the non-local scheme using Gaussian and Rician assumptions; Rajan et al. [32] proposed another scheme employing ML estimator for Rician distributed data; in Pan et al. [34] a blind local noise estimation procedure was proposed assuming that the kurtosis of the MR image is constant across different discrete cosine transformation (DCT) bands.

Unlike previously cited methodologies, there are some estimation techniques that initially calculate noise maps assuming a Gaussian distribution, and correct them to the Rician/nc-χ case for low SNRs. This correction is usually achieved by using the celebrated Koay's correction proposed in [45]. Note that all these techniques require the estimation of an extra measure, the SNR, which is also position

dependent. Sharing this strategy, Manjón et al. [31] modeled noise variance as a minimal distance between local neighborhood (patch) of the current pixel and the remaining patches in the non-local means (NLM) scheme. This approach uses the difference between noisy and the low-pass filtered image to determine local noise estimates. In a similar fashion, Borrelli et al. [37] use the difference between noisy and an NLM pre-filtered image to obtain local sample variances followed by median filtering and Rician adaptation. Maximov et al. [21] generalized the median absolute deviation (MAD) robust estimator, initially proposed for stationary Rician case by Coupé et al. [46], to estimate non-stationary noise in DTI data sets.

All the approaches reviewed so far were intended for general purpose MRI (although most of them were only tested over brain data). However, some authors took advantage of the specificity of particular acquisitions to extract the noise information. Veraart et al. [22] proposed a method very similar to the one in [21], where the MAD estimator is calculated using the information of the signal along the different diffusion-weighted images (DWIs) in a diffusion MRI acquisition. Glenn et al. [23] presented a simple estimation scheme for diffusion kurtosis imaging (DKI) using a sample variance over all the diffusion gradients followed by a bias correction and Gaussian smoothing of the raw estimates. In Ding et al. [30], a random noise in dynamic MR image series such as cardiac function imaging or blood flow velocity mapping was considered. This approach takes advantage of the temporal redundancy between acquisitions and it does not require any specific data distribution or image reconstruction technique assumptions.

In the last two years, the number of proposals for non-stationary noise estimators in literature has remarkably increased. This is a clear sign of the awareness of the importance of this task by the MRI community.

Liu et al. [36] adapted the MAD estimator to single MR images. In Dikaios et al. [5], the Koay's correction was generalized for the approximation of the sum of the Rician probability density functions (PDFs) providing the corrections for MAD in averaged diffusion images. In [19], Aja-Fernández et al. showed a comprehensive statistical noise analysis for SENSE and GRAPPA providing closed-form expressions for the non-stationary variance of noise for both modalities. They propose some techniques to estimate noise, but those methods need extra information for an accurate estimation, like the sensitivity coil profiles and the reconstruction coefficients. In a similar fashion, Hansen et al. [38] developed another scheme to measure the noise level of any linear combination of complex, magnitude, or phase pixel values of a Cartesian MRI acquisition. The method requires access to the raw MR data and additional technical details about the acquisition process.

Tabelow et al. [39] adapted the propagation-separation method to nc-χ distributed data followed by a median filter smoothing. This approach calculates spatially variant noise maps by means of the weighted ML estimator which is restricted to homogeneous regions. Aja-Fernández et al. [14] proposed a homomorphic approach to separate spatially variant noise into two terms: a stationary noise term and the low-frequency component corresponding to the noise pattern. This technique avoids the granular effect due to local estimation and leads to a simple implementation based on basic filtering—a great advantage when compared to the other methods. The homomorphic filter was further extended in [40] to blind noise estimation in GRAPPA. At the same time, Manjón et al. [41] proposed another noise estimation technique using sparseness and self-similarity properties of MR images. They utilize a principal component analysis (PCA) decomposition in the NLM scheme to extract the noisy component of the signal. The noise standard deviation is finally obtained as a median of the eigenvalues of the PCA decomposition and it is subsequently corrected to deal with the Rician case. In [42], Poot and Klein proposed a spatially regularized ML estimator to simultaneously estimate the noise pattern and diffusion tensor parameters. Finally, Veraart et al. [43] presented another scheme to estimate the spatially variant noise maps in diffusion MR imaging using the redundancy of the signal in DWI data. The method identifies the noise level using the combination of local PCA with random matrix theory.

The methodologies of the state of the art dealing with spatially variant noise are summarized in Table 1, where we specify the context in which the method was designed (image modality in the case of non-MRI images or the reconstruction method in the case of MRI, where *non-pMRI* accounts for single-coil MRI). Besides, although all methods were defined for non-stationary noise, some of them take advantage of the multidimensional nature of the acquisition to get the spatial estimation of noise in each voxel. The underlying noise model is described as well as the domain where the estimation is performed. Finally, we include if any repeated acquisition or additional data is required.

2.2 The Variance-Stabilizing Transformation

The variance-stabilizing transformation is a data transformation that has been historically applied to simplify the analysis of variance of a certain random variable whose variance is related to the mean level of the measurements [47]. The main goal of a VST is to compensate the change of the variance with respect to the change of the mean value—whenever this relationship is known—in order to provide a constant variance.

The derivation of the VST is commonly associated to the so-called *delta method*, which links the central limit theorem with the convergence of the transformed random variable $Y = f(X)$ by a differentiable function f. Formally speaking, let X_n be a sequence of random variables that satisfies $\sqrt{n}(X_n - \mu) \xrightarrow{d} \mathcal{N}(0, \sigma^2)$ (i.e., convergence in distribution). Then the first order Taylor expansion of $f(X_n)$ around μ is $f(X_n) = f(\mu) + f'(\mu)(X_n - \mu)$, which reordering terms gives

$$\sqrt{n}(f(X_n) - f(\mu)) = f'(\mu)\sqrt{n}(X_n - \mu).$$

Since X_n converges in distribution to a constant, $X_n \xrightarrow{d} \mu$, it also converges in probability and the Slutsky's Theorem [48] can be applied to ensure convergence in distribution as $f'(\mu)\sqrt{n}(X_n - \mu) \xrightarrow{d} \mathcal{N}(0, \sigma^2(f'(\mu))^2)$. Thus, we conclude

$$\sqrt{n}(f(X_n) - f(\mu)) \xrightarrow{d} \mathcal{N}(0, \sigma^2(f'(\mu))^2). \quad (1)$$

TABLE 1
Comparison of Spatially Variable Noise Estimation Techniques in MRI or Rician/nc-χ Distributed Data

Method	Year	Imaging context	Spatially variable noise	Noise assumptions	Estimation domain	Repeated acquisitions	Additional data
Marzetta [24]	1995	SAR	yes	Rician	-	-	no
DeVore *et al.* [25]	2000	SAR	yes	Rician	image	yes	no
Samsonov *et al.* [18]	2004	SENSE	yes	Gaussian	image ($\mp$)	no	yes ($\ominus$)
Goossens *et al.* [26]	2006	No pMRI, pMRI	yes	Gaussian	wavelet	no	no
Delakis *et al.* [27]	2007	SENSE	yes	Rayleigh	wavelet – image	no	no
Landman *et al.* [20], [28]	2009	SENSE	yes ($\star$)	Gaussian	image	yes ($\dagger$)	yes ($\otimes$)
Guo and Huang [29]	2009	SENSE, GRAPPA	yes	Gaussian	image ($\pm$)	no	no
Ding *et al.* [30]	2010	No pMRI, SoS, SENSE	yes	Gaussian ($\diamond$)	image	no ($\ddagger$)	no
Manjón *et al.* [31]	2010	No pMRI, SENSE GRAPPA	yes	Gaussian + Rician adaptation	image	no	no
Rajan *et al.* [32]	2011	No pMRI	yes	Rician	image	no	no
Maximov *et al.* [21]	2012	No pMRI	yes ($\star$)	Gaussian + Rician adaptation	image	yes	no
Maggioni & Foi [33]	2012	No pMRI	yes	Gaussian, Rician	image	no	no
Pan *et al.* [34]	2012	SENSE	yes	Gaussian	image	no	no
Aja-Fernández *et al.* [35]	2013	SoS	yes	nc-χ	image	no	no
Veraart *et al.* [22]	2013	SENSE, SoS	yes ($\star$)	Gaussian + Rician/nc-χ adaptation	wavelet	yes ($\times$)	no
Aja-Fernández *et al.* [19]	2014	SENSE, GRAPPA, SoS	yes	Rayleigh, c-χ	image	no	yes ($\odot$)
Liu *et al.* [36]	2014	No pMRI, SENSE	yes	Gaussian + Rician adaptation	wavelet	no	no
Borrelli *et al.* [37]	2014	SENSE, GRAPPA	yes	Gaussian + Rician adaptation	image	no	no
Dikaios *et al.* [5]	2014	SENSE, GRAPPA	yes ($\star$)	Gaussian + Rician adaptation	wavelet	yes	no
Glenn *et al.* [23]	2015	No pMRI	yes ($\star$)	Rician	image	yes	no
Hansen *et al.* [38]	2015	pMRI ($\div$)	yes	Gaussian	image	no	yes ($\oslash$)
Aja-Fernández *et al.* [14]	2015	SENSE	yes	Gaussian, Rayleigh, Rician	image	no	no
Tabelow *et al.* [39]	2015	SENSE, GRAPPA, zoomed GRAPPA	yes	nc-χ	image	no	no
Aja-Fernández *et al.* [40]	2015	GRAPPA	yes	Gaussian	wavelet	no	no
Manjón *et al.* [41]	2015	SENSE	yes	Gaussian + Rician adaptation	image	no	no
Poot & Klein [42]	2015	No pMRI, SENSE	yes ($\star$)	Rician	image	no	no
Veraart *et al.* [43]	2016	GRAPPA	yes ($\star$)	Gaussian + nc-χ adaptation ($\diamond$)	image	no ($\times$)	no
Our proposal		SENSE	yes	Rician	image	no	no

($\div$) The method can measure the noise level for any linear combination of pixels in an MR image.
($\ominus$) Additional samples of the air background are required for SENSE.
($\mp$) Noise level is represented as a local conductance parameter in the anisotropic diffusion filter.
($\dagger$) A biophysical model of the imaging data is required.
($\star$) Noise is spatially measured with samples from different acquisitions, (e.g. different gradients in DTI).
($\odot$) Sensitivity maps for SENSE; reconstruction coefficients and correlations for GRAPPA are required.
($\times$) Method uses the information of different DWIs to estimate the noise.
($\diamond$) The eigenvalues of the covariance are assumed to be Marchenko-Pastur distributed.
($\pm$) Noise level is estimated indirectly as a smoothing weight in the total variation regularization.
($\otimes$) Multiple contrast type signals and a coil sensitivity model are required.
($\ddagger$) Method intended for successive dynamic image series rather than repeated acquisitions.
($\oslash$) The image reconstruction matrix, sampling pattern and the complex images are required.

Now, let us suppose that the variance depends on the mean value, $\sigma^2 = \mathrm{Var}(\mu)$. We are interested in finding a transformation $f(\cdot)$ such that $\sigma^2(f'(\mu))^2$ is a constant. For that purpose, the following differential equation can be set: $\sigma^2(f'(\mu))^2 = C^2$, whose solution provides the expression commonly used to calculate the VST [47]

$$f(x) = \int^x \frac{C}{\sqrt{\mathrm{Var}(\mu)}} d\mu, \tag{2}$$

where C is arbitrary constant.

The VST has lately gained importance in the image processing field. In the case of MRI, this methodology has mainly focused on signal-dependent noise estimation and removal procedures [49], [50]. In the case of Rician distributed data, the problem of stabilizing its variance stems from its functional dependence with the mean. In [49], Foi derived an asymptotic stabilizer for Rician data considering the asymptotic approximation of the variance for large values of A in the following way.

Let M denote a Rician random variable (RV) with noncentrality parameter A and scale parameter σ (i.e., $M \sim \mathrm{Rice}(A, \sigma)$), whose PDF is defined as

$$p(M|A,\sigma) = \frac{M}{\sigma^2}\exp\left(-\frac{M^2+A^2}{2\sigma^2}\right) I_0\left(\frac{MA}{\sigma^2}\right), \quad M \geq 0, \tag{3}$$

where $I_0(\cdot)$ is the modified Bessel function of the first kind and zeroth order.

The functional dependence of the variance of M for large values of A is $\mathrm{Var}\{M|A,\sigma\} \approx \sigma^2 - \frac{\sigma^4}{2A^2}$. Thus, by means of Eq. (2), the asymptotic stabilizer of the Rician RV becomes

$$f_{\mathrm{stab}}(M|\sigma) = \sqrt{\frac{M^2}{\sigma^2} - \frac{1}{2}} + a, \quad a \in \mathbb{R}, \tag{4}$$

with $M \geq \frac{\sigma}{\sqrt{2}}$ and a an arbitrary constant.

Due to the asymptotic derivation of Eq. (4), this result is valid for high SNR areas, though it no longer applies for lower ratios ($\mathrm{SNR} < 5$). To properly handle low SNRs, Foi proposed in [49] a numerical stabilization which accounts for smoothness and asymptotic convergence of Eq. (4). During the optimization procedure, the constraints are weighted with different configurations giving two different stabilizers that, for the sake of comparison, will be denoted as Foi's model A and Foi's model B. The numerical optimization applied requires the estimation of the σ parameter to stabilize the RV, which is iteratively refined by means of an algorithm based on the fixed-point theorem (see [49] for more details).

Foi's method proved its suitability for single-coil systems, where the noise is assumed to be stationary. However, a problem arises in the case of non-stationary Rician data, since the estimation of σ must be done locally, i.e., $\sigma(\mathbf{x})$. The

direct implication is a considerable reduction of the number of samples available for local estimation and, thus, the accuracy of the estimation is consequently reduced. This leads to an inaccurate estimator of $\sigma(\mathbf{x})$, especially near edges, which results in a poor stabilization.

It is important to note that other transformations could be proposed in order to transform a Rician distributed RV to a Gaussian variate. For instance, in [51] Koay et al. used the well-known *inverse transform method* also known as the *quantile-quantile transformation*, which maps the quantiles from the original data to the quantiles of a Gaussian RV. This is achieved by using the cumulative distribution function (CDF) of the Rician RV, $F_M(\cdot|A,\sigma)$, and then applying the inverse CDF of a Gaussian RV as follows:

$$M_G = F_{M_G}^{-1}\big(F_M(M|A,\sigma)\big|A,\sigma\big), \tag{5}$$

where $F_{M_G}^{-1}(\cdot|A,\sigma)$ is the inverse CDF of a Gaussian RV with the expectation A and the standard deviation σ. This approach requires the parameters of Rician signal to be known in advance to apply the transformation. The resulting Gaussian distribution strongly depends on the estimation of the mean and variance and becomes less robust than the VST as we will see in the following sections.

2.3 Goals of the Proposed Methodology

Attending to the main characteristics of the aforementioned techniques we propose a methodology that provides the same advantages of them but also overcomes their limitations. The methodology we pursue should show the following features:

1) *No Granularity*. It should avoid granular patterns in the estimation due to inaccurate estimates near the edges or inhomogeneities in tissues.
2) *Robustness for all SNRs*. Some methods rely on the asymptotic behavior of Rician RVs and are just applicable for high SNRs. Others such as the inverse transformation method strongly depend on accurate estimates. These assumptions may cause an undesired bias that may result in an inaccurate estimate of noise when SNR is low.
3) *No need of extra information*. We want to keep the methodology as simple as possible in order to avoid information that is not usually available in conventional acquisitions (repeated acquisitions, multiple contrast images, biophysical models, background or foreground region extraction).

3 Non-Stationary Rician Noise Estimation

In this section, we propose a methodology especially designed to meet the aforementioned features by defining a function that maps non-stationary Rice data to its stationary Gaussian distributed counterpart. This function is inspired by the VST theory already presented. Finally, the data can be stabilized by performing a suitable homomorphic filtering that estimates the non-stationary noise map without granular patterns.

It is important to note that the proposed transformation does not fall into the field of VST in the classical sense, in which the transformation is obtained by considering the differential equation resulting from the delta method. Instead, we propose to extend the stabilization function obtained by the classical VST equation, Eq. (2), to a more general case in which low SNRs are also considered. This is achieved by introducing two degrees of freedom by means of a versatile parametric form derived from Eq. (4). This way, the proposed formulation links the philosophy of the *inverse transform method*, which is not subject to constraints on the SNRs, to the asymptotic approach obtained with the VST theory. This implies that an estimate of the SNR is required and, though it could seem as an inconvenience, we will show that both the initialization of σ and the estimation of the SNR per pixel can be efficiently achieved avoiding the main problems of other estimators. Besides, this formulation shows some important advantages: 1) It stabilizes the whole range of SNRs; 2) Is a single-shot transformation that does not need an iterative estimation of σ.

3.1 Whole Range Variance-Stabilizer Transform

First, we propose the parametrization of the stabilization transformation shown in Eq. (4) using a vector parameter $\mathbf{\Theta} = (\theta_1, \theta_2)$ as follows:

$$f_{\text{stab}}(M|\sigma,\mathbf{\Theta}) = \sqrt{\max\left\{\theta_1^2\frac{M^2}{\sigma^2} - \theta_2,\ 0\right\}}. \tag{6}$$

Note that when $(\theta_1,\theta_2) = (1, 0.5)$, Eq. (6) becomes the asymptotic solution of Eq (4).

In order to cope with the different behaviors of the stabilizer as a function of the SNR, the parameters should be tuned conveniently. This can be efficiently achieved by using a numerical optimization procedure with the following optimization criterion

$$\mathbf{\Theta}_{\text{opt}} = \arg\min_{\mathbf{\Theta}}\ J(f_{\text{stab}}(M|\sigma,\mathbf{\Theta})), \tag{7}$$

with $\mathbf{\Theta}_{\text{opt}} = (\theta_{1\text{opt}}, \theta_{2\text{opt}})$ and $J:\mathbb{R}^2 \mapsto \mathbb{R}$ being a cost function to be minimized

$$\begin{aligned} J(f_{\text{stab}}(M|\sigma,\mathbf{\Theta})) = {} & \lambda_1 \cdot (1 - \text{Var}\{f_{\text{stab}}(M|\sigma,\mathbf{\Theta})\})^2 \\ & + \lambda_2 \cdot (\text{Skewness}\{f_{\text{stab}}(M|\sigma,\mathbf{\Theta})\})^2 \\ & + \lambda_3 \cdot (\text{ExcessKurtosis}\{f_{\text{stab}}(M|\sigma,\mathbf{\Theta})\})^2, \end{aligned} \tag{8}$$

Note that the cost function favors a unitary variance, zero skewness and zero excess of kurtosis,[1] enforcing the desired Gaussian behavior of the transformed RV.

The selection of parameter $\Lambda \in \mathbf{\Lambda}\{(\lambda_1,\lambda_2,\lambda_3) \in [0,1]^3 : \lambda_1+\lambda_2+\lambda_3 = 1\}$ was done empirically by following the *minimum distance estimation* criterion, where the distance d was induced from the supremum norm as

$$\widehat{\Lambda} = \arg\inf_{\Lambda}\{d = ||F_{\mathcal{N}} - \widehat{F}(J(f_{\text{stab}}(\mathbf{x}|\sigma,\mathbf{\Theta}_{\text{opt}}),\Lambda))||_\infty : \Lambda \in \mathbf{\Lambda}\}, \tag{9}$$

where $\mathbf{x} = [x_1,\ldots,x_n]$ are Rician distributed samples; $F_{\mathcal{N}}$ is the CDF of a standardized Gaussian distribution, $\mathcal{N}(0,1)$; $\widehat{F}(\mathbf{y})$ is the empirical CDF of samples in $\mathbf{y}$. The values for λ_2 and λ_3 were set equal but smaller than λ_1 to ensure the

1. The Kurtosis of a Gaussian random variable is 3.

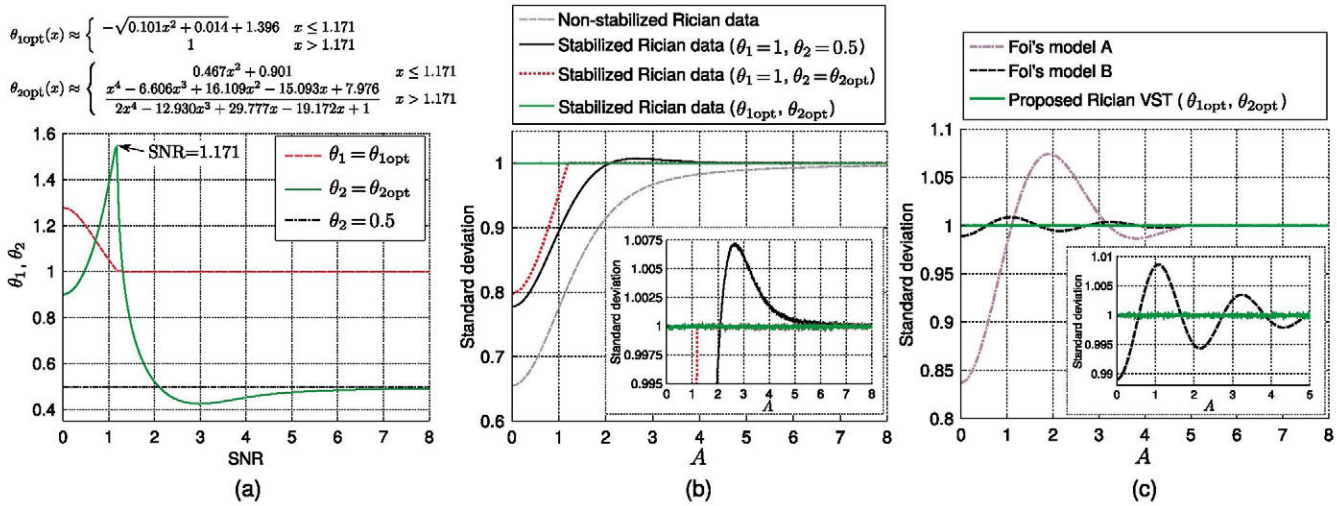

Fig. 1. (a) Optimized parameters θ_{1opt} and θ_{2opt} in terms of SNR and their closed-form approximations, (b) comparison of standard deviations between Rician distributed data and different stabilizing transforms, (c) standard deviation of the variance-stabilizing parametric approach $f_{stab}(M|\sigma, \Theta_{opt})$ compared to Foi's stabilizers.

stabilization. Eventually, the configuration was set to $\lambda_1 = 0.998$, $\lambda_2 = \lambda_3 = 0.001$.

The numerical optimization of Eq. (7) is carried out for each SNR step, $\sigma = 1$ and A between 0.001 and 20 (logarithmically increasing) by means of the Nelder-Mead method. Variance, skewness and kurtosis are calculated in terms of the rth raw moments of the transformed RV

$$\begin{aligned} \mathrm{Var}\{f_{stab}(M|\sigma,\Theta)\} &= m_2 - m_1^2, \\ \mathrm{Skew}\{f_{stab}(M|\sigma,\Theta)\} &= \frac{m_3 - 3m_1m_2 + 2m_1^3}{(m_2 - m_1^2)^{\frac{3}{2}}}, \\ \mathrm{Kurt}\{f_{stab}(M|\sigma,\Theta)\} &= \frac{m_4 - 4m_1m_3 + 6m_1^2m_2 - 3m_1^4}{(m_2 - m_1^2)^2}, \end{aligned}$$

where

$$m_r = \int_0^\infty f_{stab}^r(M|\sigma,\Theta)p(M|A,\sigma)dM,$$

is calculated by means of the adaptive Gauss-Kronrod quadrature in the interval $M \in [0, 30]$.

The optimal values of θ_1 and θ_2 obtained according to Eq. (7) for different SNRs (with $\mathrm{SNR} = A/\sigma$) are shown in Fig. 1a jointly to their closed-form approximations. Besides, in Fig. 1b we show the standard deviations of non-stabilized and stabilized data for different sets of optimized parameters. Note that the stabilization obtained with the asymptotic solution, $(\theta_1, \theta_2) = (1, 0.5)$, slightly improves when the optimal value θ_{2opt} is considered, though it still lacks of good stabilization for small SNR (where the Rayleigh assumption holds). Conversely, the optimal set of parameters $(\theta_{1opt}, \theta_{2opt})$ show an outstanding stabilization through the whole SNR range as was desired. In Fig. 1c, the proposed parametric form of VST is compared to Foi's models [49].

3.2 Spatially Variant Noise Estimation

We propose a new methodology to estimate the non-stationary noise out of Rician data, following the pipeline summarized in Fig. 2. The strength of this methodology lies in a proper stabilization of the Rician image for all SNRs that allows the subsequent processing of the data as Gaussian. The first step of the process is the application of the parametric VST to the magnitude MR image, which transforms the non-stationary Rician data to a stationary Gaussian-like distributed data. A prior estimation of the SNR and the variance of noise will be needed as input parameters. Once the data is stabilized, we can use a non-stationary Gaussian noise estimator to extract the variance of noise from the image. In this work, we will make use of the Gaussian homomorphic approach proposed in [14], since it has proved its accuracy and robustness. In what follows, we analyze each step separately.

First, the aforementioned parametric VST is applied to the noisy magnitude MR image $I(\mathbf{x})$

$$\widetilde{I}(\mathbf{x}) = \widehat{\sigma_0(\mathbf{x})} \cdot f_{stab}\Big(I(\mathbf{x})|\widehat{\sigma_0(\mathbf{x})}, \theta_{1opt}(\mathbf{x}), \theta_{2opt}(\mathbf{x})\Big), \qquad (10)$$

where $\widehat{\sigma_0(\mathbf{x})}$ is the prior noise map, $\theta_{1opt}(\mathbf{x})$ and $\theta_{2opt}(\mathbf{x})$ are the optimized to local SNR transformation parameters

$$\theta_{1opt}(\mathbf{x}) = (\theta_1 \circ \mathrm{SNR})(\mathbf{x}),\ \theta_{2opt}(\mathbf{x}) = (\theta_2 \circ \mathrm{SNR})(\mathbf{x}), \qquad (11)$$

with pointwise SNR defined as $\mathrm{SNR}(\mathbf{x}) = \frac{A(\mathbf{x})}{\sigma(\mathbf{x})}$. Note that the stabilization needs an estimate of both the SNR and σ for each location. Many of the methods in literature can be used for that purpose. In this work, we use the local mean of the image $I(\mathbf{x})$ as the estimate of the underlying signal $\widehat{A(\mathbf{x})}$ in a square window and the noise estimate provided in [14]. This simple strategy avoids granularities of the SNR map usually provided by other methods. However, any method discussed in Section 2.1 can be used to calculate $\widehat{\sigma(\mathbf{x})}$. In the

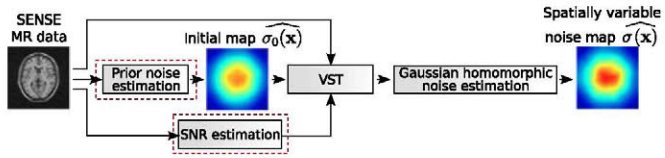

Fig. 2. General scheme of the proposed non-stationary Rician noise estimation algorithm. The red rectangles indicate interchangeable modules of the algorithm.

experimental section, we will show the performance of each initialization and we will justify our choice.

Using the proposed parametric VST, Eq. (10) reads

$$\widetilde{I}(\mathbf{x}) = \widehat{\sigma_0(\mathbf{x})}\sqrt{\max\left\{\theta_{1\text{opt}}^2(\mathbf{x})\frac{I^2(\mathbf{x})}{\widehat{\sigma_0^2(\mathbf{x})}} - \theta_{2\text{opt}}(\mathbf{x}),\ 0\right\}}, \quad (12)$$

where $\widetilde{I}(\mathbf{x})$ is the stabilized image multiplied by the initial noise map estimate $\widehat{\sigma_0(\mathbf{x})}$. After the stabilization, this image is assumed to be a noise-free component $A(\mathbf{x})$ corrupted with additive Gaussian distributed noise $N(\mathbf{x}; 0, \sigma^2(\mathbf{x}))$ with zero mean and spatially variable variance $\sigma^2(\mathbf{x})$

$$\widetilde{I}(\mathbf{x}) \approx A(\mathbf{x}) + N(\mathbf{x}; 0, \sigma^2(\mathbf{x})) = A(\mathbf{x}) + \sigma(\mathbf{x}) \cdot N(\mathbf{x}; 0, 1). \quad (13)$$

This is the same assumption considered in [49], [52]. In the experiments section, we will show that it perfectly holds for the whole range of SNRs.

In the *second* stage, we need to separate the low-frequency noise map $\sigma(\mathbf{x})$ from Eq. (13). To do so we adopt the homomorphic approach proposed in [14], where a log transformation is first applied to the centered data. To center the data, we remove the mean to the signal

$$\widetilde{I}_{\text{C}}(\mathbf{x}) = \widetilde{I}(\mathbf{x}) - \mathbb{E}\{\widetilde{I}(\mathbf{x})\} = \sigma(\mathbf{x}) \cdot N(\mathbf{x}; 0, 1), \quad (14)$$

where $\mathbb{E}\{\cdot\}$ is the (local) expectation operator applied to the variance-stabilized image. $\mathbb{E}\{\cdot\}$ must be approximated for practical implementation. One straight forward approximation would be the local average in a neighborhood as was done in [14]. However, this method is prone to provide inaccurate estimates due to the presence of different tissues within the local window. Once more, different methods from literature could be used here. In this paper, we consider two edge-preserving algorithms: the bilateral filter for grayscale images proposed in [53] and the SWT [22].

The bilateral filter is applied to the magnitude of variance-stabilized MR image $\widetilde{I}(\mathbf{x})$ as follows:

$$\Psi(\mathbf{x}) = \frac{\sum_{\mathbf{p}\in\eta(\mathbf{x})} \psi_{\sigma_{\text{g}}}(\|\mathbf{p}-\mathbf{x}\|)\psi_{\sigma_{\text{r}}}(|\widetilde{I}(\mathbf{p}) - \widetilde{I}(\mathbf{x})|)\widetilde{I}(\mathbf{p})}{\sum_{\mathbf{p}\in\eta(\mathbf{x})} \psi_{\sigma_{\text{g}}}(\|\mathbf{p}-\mathbf{x}\|)\psi_{\sigma_{\text{r}}}(|\widetilde{I}(\mathbf{p}) - \widetilde{I}(\mathbf{x})|)}, \quad (15)$$

where $\eta(\mathbf{x})$ is a neighborhood of pixel $\mathbf{x}$, $\psi_{\sigma_{\text{g}}}$ and $\psi_{\sigma_{\text{r}}}$ are geometric and radiometric distances [53]. In our case, $\psi_{\sigma_{\text{g}}}$ and $\psi_{\sigma_{\text{r}}}$ are defined as $\psi_{\sigma_{\text{r}}} = \psi_{\sigma_{\text{g}}}(x) = \exp(-\frac{x^2}{2\sigma_{\text{g}}^2})$. Therefore, the centered data can be calculated by $\widetilde{I}_{\text{C}}(\mathbf{x}) = \widetilde{I}(\mathbf{x}) - \Psi(\mathbf{x})$.

Alternatively, this task can be done by an SWT, which directly centers the data, since it extracts the noise component from $\widetilde{I}(\mathbf{x})$ using the high-high (HH) subband of SWT algorithm at scale $s = 1$. Specifically, the noise component corresponds to the diagonal detail coefficients

$$\widetilde{I}_{\text{C}}(\mathbf{x}) = ((\widetilde{I} \circledast g^{(r)}) \circledast g^{(c)})(\mathbf{x}), \quad (16)$$

where the convolution procedure is performed with a separable one-dimensional high-pass filter g (i.e., $g^{(r)}$ convolves along the rows and $g^{(c)}$ along the columns).

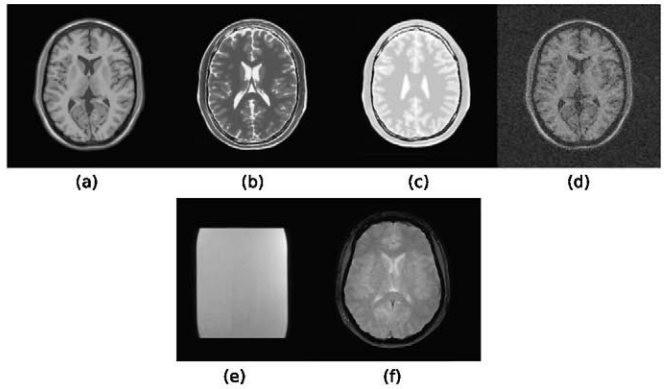

Fig. 3. Data sets used in the experiments: (a) synthetic noise-free T_1-, (b) T_2- and (c) PD-weighted MR data, (d) synthetic noisy T_1-weighted SENSE simulated image, (e) real noisy T_1-weighted SENSE phantom and (f) *in vivo* T_2-weighted FFE SENSE brain data.

Once the data is centered, the logarithm is applied

$$\log|\widetilde{I}_{\text{C}}(\mathbf{x})| = \underbrace{\log\sigma(\mathbf{x})}_{\text{low frequency}} + \underbrace{\log|N(\mathbf{x}; 0, 1)|}_{\text{high frequency}}.$$

Since the multiplicative character of the noise can be represented as two additive components, we can separate the low-frequency component by simple low-pass filtering

$$\text{LPF}\left\{\log\left|\widetilde{I}_{\text{C}}(\mathbf{x})\right|\right\} \approx \log\sigma(\mathbf{x}) - \text{LPF}\{\log|N(\mathbf{x}; 0, 1)|\}, \quad (17)$$

where LPF is a low-pass filter. Thus, considering that $|N(\mathbf{x}; 0, 1)|$ follows a half-Gaussian distribution and assuming that we can consider the LPF as a good approximation of the mean, we can write

$$\text{LPF}\left\{\log\left|\widetilde{I}_{\text{C}}(\mathbf{x})\right|\right\} \approx \log\sigma(\mathbf{x}) - \log\sqrt{2} - \frac{\gamma}{2}, \quad (18)$$

with γ being the Euler-Mascheroni constant.

Finally, Eq. (18) leads to a spatially variant noise estimator defined as follows:

$$\widehat{\sigma(\mathbf{x})} \approx \sqrt{2}e^{\text{LPF}\left\{\log\left|\widetilde{I}_{\text{C}}(\mathbf{x})\right|\right\} + \frac{\gamma}{2}}. \quad (19)$$

4 Materials and Methods

In this section, we introduce the MR data used in the validation process of the proposal and the characterization of extra parameters used by evaluated state-of-the-art techniques in non-stationary Rician noise estimation.

4.1 Materials

The following data sets are used for comparison:

- *Synthetic MRI:* three MR slices from BrainWeb simulated database [54] at different transverse planes (T_1-, T_2- and PD-weighted MR data) all with intensity non-uniformity INU = 0 percent. The data is free of noise, the background areas are set to zero, the slice thickness is 1 mm and the intensity range normalized to [0–255] (Figs. 3a, 3b, and 3c).
- *Artificial noise patterns:* four different spatially variant noise maps normally observed in real pMRI acquisitions of the brain [19], [20], [31] (Fig. 4).

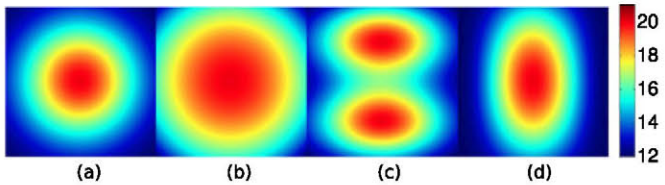

Fig. 4. Spatially variant noise patterns used in the experiments for synthetic MRI.

- *Synthetic SENSE MRI:* a synthetic T_1-weighted image from BrainWeb database is used to simulate the Cartesian SENSE data reconstructed from eight receiver coils ($L = 8$), reduction factor $r = 2$, correlations $\rho_{i,j} = 0.2$ between coils and variance of the noise $\sigma_l^2(\mathbf{x}) = 75$ per coil (Fig. 3d).
- *Real SENSE MR phantom:* twenty repetitions of T_1-weighted scan of a doped ball phantom were performed using Philips Achieva 3.0T TX device provided with a 32-channel coil system using Turbo Field Echo (TFE) sequence, volume size $224 \times 224 \times 59$, TR = 5.264 ms/TE = 2.569 ms, slice thickness 3.20 mm, and reduction factor $r = 2$ (Fig. 3e).
- *In vivo SENSE MR brain data*: T_2-weighted scan of the brain in transverse plane was acquired using Fast Field Echo (FFE) sequence.[2] The volume size equals $240 \times 180 \times 161$, TR = 3,000 ms/TE = 80 ms, slice thickness 3.20 mm and the reduction factor $r = 4$ (Fig. 3f).

The noise patterns are adapted to the synthetic images by adding complex Gaussian noise to the x-space domain of the phantom and then the final noisy image is given by

$$I(\mathbf{x}) = |A(\mathbf{x}) + N_{\text{re}}(\mathbf{x}) + j \cdot N_{\text{im}}(\mathbf{x})|, \tag{20}$$

where $A(\mathbf{x})$ is a noise-free MRI and $N_{\text{re}}(\mathbf{x}), N_{\text{im}}(\mathbf{x}) \sim \mathcal{N}(0, \sigma^2(\mathbf{x}))$ are uncorrelated Gaussian distributed noise with scale parameter $\sigma^2(\mathbf{x})$ varying across the image.

The accuracy of noise estimators in synthetic experiments is evaluated using the pointwise relative error (RE) of an estimate $\widehat{\sigma_i(\mathbf{x})}$ for ith repetition of the experiment, $\text{RE}_i(\mathbf{x})$, and then averaged along R repetitions

$$\text{RE}_i(\mathbf{x}) = \frac{\left|\widehat{\sigma_i(\mathbf{x})} - \sigma(\mathbf{x})\right|}{\sigma(\mathbf{x})}, \qquad \text{RE}(\mathbf{x}) = \frac{1}{R}\sum_{i=1}^{R} \text{RE}_i(\mathbf{x}). \tag{21}$$

For quantitative numerical evaluations, the parameter $\text{RE}(\mathbf{x})$ is averaged across the foreground area of the image to get one single value for a given SNR level.

Furthermore, we define the variance (VAR) of the parameter $\text{RE}(\mathbf{x})$ as follows:

$$\text{VAR}(\mathbf{x}) = \frac{1}{R-1}\sum_{i=1}^{R} (\text{RE}_i(\mathbf{x}) - \text{RE}(\mathbf{x}))^2. \tag{22}$$

Similarly, we spatially average $\text{VAR}(\mathbf{x})$ in the foreground area of the image to get the variance of the estimator.[3]

4.2 Methods

For the sake of comparison, we used the 14 noise estimation techniques included in Table 1 and described in Section 2.1. All these methods can be directly applied to retrospectively reconstructed single MR slices. The implementation was done in MATLAB, except Tabelow's method [39], whose source code in GNU R was provided by authors.[4] For Maggioni and Foi [33] and Aja-Fernández et al. [14] we used the code downloaded from the their websites.[5,6] The code of our proposed method is available at.[7]

Below, we give a brief description of the parameters used by the state-of-the-art methods:

- DeVore et al. [25]: 10 iterations.
- Delakis et al. [27]: the Daubechies 7 (db7) wavelet was used for SWT decomposition.
- Maximov et al. [21]: the Koay correction uses 5×5 window size for local SNR estimation.
- Liu et al. [36]: the db7 wavelet was used for SWT and Koay correction with 5×5 windows.
- Goossens et al. [26]: db7 wavelet was used for SWT.
- Landman et al. [20]: the biophysical model is obtained as the NLM pre-filtered image for size 5×5 and 11×11 (local and search windows).
- Manjón et al. (2010) [31]: data is smoothed in 3×3 windows, the NLM filter uses 5×5 and 11×11 windows, the Koay correction uses 5×5.
- Rajan et al. [32]: It uses a 11×11 windows for ML and the threshold for tissue classification is obtained from a histogram with 1,000 bins.
- Pan et al. [34]: It uses 8×8 DCT basis and local moments are calculated in 5×5 windows.
- Maggioni and Foi [33]: algorithm uses standard parameters recommended by the authors.
- Borrelli et al. [37]: NLM filter uses 5×5 and 11×11 windows, the Koay correction and median smoothing are obtained with 5×5 windows.
- Tabelow et al. [39]: 10 iterations were applied and parameters recommended by the authors.
- Manjón et al. (2015) [41]: NLM scheme uses 5×5 and 11×11 windows, trimmed median as a noise estimator, and smoothing of the raw estimates with 11×11 windows.
- Aja-Fernández et al. [14]: the EM algorithm is used to extract a noise component for T_1-weighted MR data and the SWT with db7 wavelet is applied for T_2- and PD-weighted MR data, the low pass filter is set to $\sigma_f = 3.4$,
- The proposal: the SWT uses db7 wavelet and the edge-preserving bilateral filter with 5×5 windows, the low pass filter is implemented as a Gaussian filter in the frequency domain with a variance of $\sigma_f = 3.4$.

The selection of parameters was done by using those suggested in the original papers and, whenever those parameters have the same meaning (local and search windows, estimation windows) we use the same parameters.

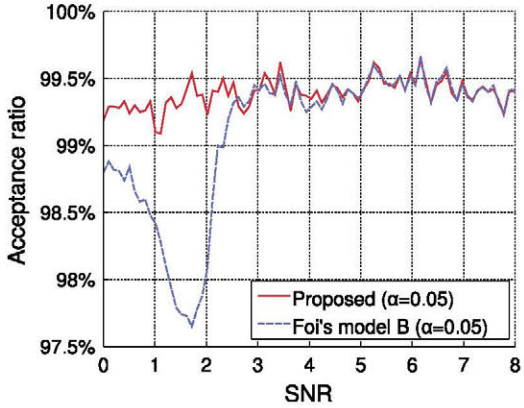

Fig. 5. Anderson-Darling test of Gaussianity for the noise component in variance-stabilized MR signal.

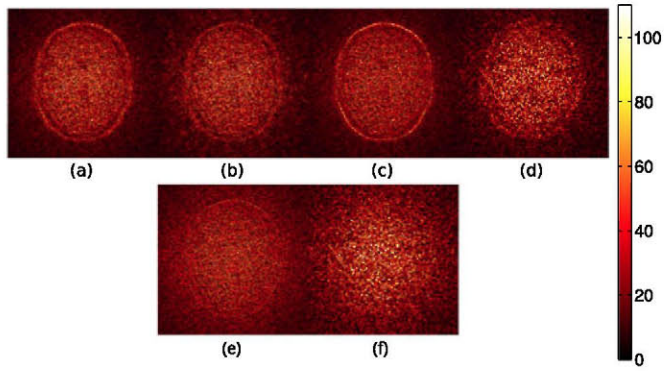

Fig. 6. Noise component extracted with different techniques: (a) local mean, (b) local EM algorithm, (c) bilateral filter, (d) HH subband of SWT, (e) VST + bilateral filter (proposed), (f) VST + HH subband of SWT (proposed).

5 Experimental Results and Discussion

In this section we compare our proposal with the aforementioned state-of-the-art techniques for non-stationary Rician noise estimation. We carry out several experiments in the synthetic and real MRI datasets.

5.1 Statistical Analysis of the Underlying Assumption

Before testing the quantitative and qualitative performance of the method, we verify the underlying assumption of Gaussianity of the stabilized noise with an Anderson-Darling test. To extract the noise component from the stabilized signal, we apply the SWT decomposition using a high-pass filter with the db7 wavelet. We perform 10^4 independent trials of the Anderson-Darling test for each SNR step with sample size $N = 256$ and a significance level $\alpha = 0.05$. The comparison is performed with Foi's model B since it has better performance than Foi's model A. Results are depicted in Fig. 5 where one can see that the proposal overcomes Foi's model B for low SNR and it obtains at least 99.1 percent of the null hypothesis (being Gaussian) acceptances.

Finally, we visually compare the noise components extracted from stabilized and non-stabilized T_1-weighted brain MRI. For this purpose, the noise-free image was corrupted with the first pattern of Fig. 4 by means of Eq. (20) with maximum value of SNR in foreground area of the image given by $\mathrm{SNR}_{\max} = 7.68$. Now, following the underlying assumptions, the proposed VST should change the character of the noise component to AWGN and therefore it allows applying Gaussian-dedicated noise extraction procedures such as SWT decomposition. In Fig. 6, we show the noise extraction with and without VST. The presence of brain edges confirms that the methods applied to the non-stabilized image cannot successfully extract the noise from the signal (Figs. 6a and 6b shows the noise extraction from [14] and Fig. 6d from [40]), whereas the proposed methods applied to stabilized image retrieve a noise estimate without interactions of the signal (Figs. 6e and 6f).

The results obtained from these experiments evidence: 1) the assumption of Gaussianity after stabilizing the Rician data by the proposed VST still holds for low SNRs, 2) Gaussian-driven methods can be used to recover the noise component from variance-stabilized Rician data, 3) With this stabilization, post-correction factors like [14], [41], [45] are no longer required for Rician RVs.

5.2 Robustness Analysis

The sensitivity to SNR mismatch was studied in a set of Rician distributed images of size 256×256 with SNRs in the range $[0, 8]$, which were conveniently stabilized with the proposed VST. The SNR mismatch was intentionally introduced between -100 and $+100$ percent.

The resulting standard deviation of the stabilized data is shown in Fig. 7 for each SNR and mismatch. The contour lines describe the over/underestimation of the stabilized standard deviation. Note that this picture shows that a ± 25 percent of SNR mismatch produces around 7 percent of error in the stabilized standard deviation. This means that any estimation methodology proposed in the state of the art can be effectively used as the initial guess, $\widehat{\sigma_0(\mathbf{x})}$, and we expect to remarkably improve the accuracy with our methodology.

Now, we extend this experiment to check the improvement of the proposed methodology when the 14 methods described in Section 4.2 are used as the initialization. We considered a synthetic T_1-weighted brain MR image with the noise pattern shown in Fig. 4a. Four $\mathrm{SNR}_{\max}$ levels and 100 repetitions for each $\mathrm{SNR}_{\max}$ level were used.

The averaged relative errors of the proposed noise estimation scheme are shown in Table 2 with respect to

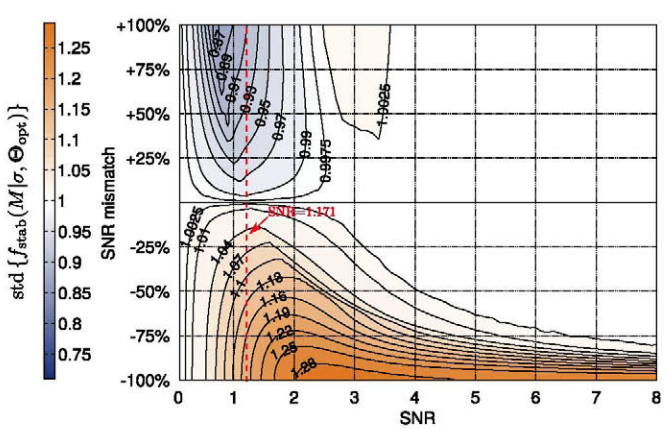

Fig. 7. Influence of SNR mismatch on standard deviation of variance-stabilized Rician data for Θ_{opt}. The red dashed line indicates the breakdown point of the parameter $\theta_{2\mathrm{opt}}$.

TABLE 2
Averaged Relative Errors of the Proposed Scheme Using Different State-of-the-Art Techniques to Initialize $\sigma_0(\mathbf{x})$

Method to estimate $\sigma_0(\mathbf{x})$	SNR_{max} 5.63	8.71	11.79	14.87
DeVore	4.77 (17.6)	4.41 (19.1)	4.46 (23.3)	4.53 (29.6)
Delakis	4.53 (16.8)	4.59 (21.2)	4.48 (23.9)	4.41 (26.2)
Maximov	4.60 (19.7)	4.48 (20.8)	4.45 (22.1)	4.36 (23.7)
Liu	4.62 (27.0)	4.64 (27.1)	4.41 (26.9)	4.35 (26.7)
Goossens	5.52 (22.8)	4.93 (20.7)	4.81 (20.0)	4.51 (19.7)
Landman	5.23 (18.5)	4.80 (16.4)	4.68 (15.5)	4.37 (15.4)
Manjón (2010)	4.56 (13.3)	4.20 (12.9)	4.23 (12.5)	4.03 (12.2)
Rajan	5.83 (20.0)	5.07 (16.9)	4.60 (15.8)	4.57 (17.7)
Pan	6.09 (25.1)	5.16 (18.6)	4.93 (15.2)	4.54 (13.0)
Maggioni/Foi	5.57 (19.2)	4.81 (12.2)	4.66 (9.2)	4.35 (8.2)
Borrelli	4.53 (11.3)	4.19 (11.6)	4.25 (11.9)	4.03 (12.1)
Tabelow	6.18 (15.7)	5.56 (10.8)	5.42 (9.9)	5.03 (10.2)
Manjón (2015)	4.64 (9.2)	4.31 (7.4)	4.37 (6.9)	4.13 (6.7)
Aja-Fernández	**4.51** (12.5)	**4.1** (10.9)	**4.15** (9.3)	**3.9** (7.7)
$\widehat{\sigma_0(\mathbf{x})} = \sigma(\mathbf{x})$	4.17	3.95	4.11	3.87

Notation: VST (w/o VST) %. The best performance for each SNR_{max} *is in bold letters.*

the results obtained from the method used for the initialization (shown in parentheses). Note that the proposal is able to estimate the final noise map even if the prior estimation provides inaccurate results (around 15 percent of SNR mismatch). Moreover, the average relative error is nearly constant among all verified methods and SNR_{max} levels, obtaining an accuracy about 5 percent, close to the error that would be obtained with an ideal estimate $\widehat{\sigma_0(\mathbf{x})} = \sigma(\mathbf{x})$. Note that the highest Relative Error obtained with the VST method is always lower than the best result obtained with any of the state-of-the-art methods. These results confirm the robustness of the method for $\sigma_0(\mathbf{x})$ mismatch and its better behavior when compared to the rest methods.

According to the results obtained in Table 2, it seems that the best option for a suitable initialization is the one provided by Aja-Fernández's [14]. This is mainly because the proposed methodology takes advantage of the smooth solution and the better estimate of the SNR provided in [14]. Thus, in what follows, we adopt the Aja-Fernández's method as the initialization step for our proposed methodology. However, our method is not confined to this initialization and any other method could be used with good results.

We finally evaluate the propagation of the mismatch error in σ throughout the proposed transformation against the inverse transform method (QQ mapping) of Eq. (5). We show in Fig. 8 the relative error calculated as the average of 2,000 independent experiments. Note that the proposed VST is systematically more robust than the inverse transform method. Both curves converge to the same values as the Rician RV converges to a Gaussian RV, i.e., SNR $\rightarrow \infty$.

5.3 Synthetic MRI Experiments

As a *first experiment*, we compare quantitatively the proposed variance-stabilizing homomorphic filter with the aforementioned methods using synthetic T_1-, T_2- and

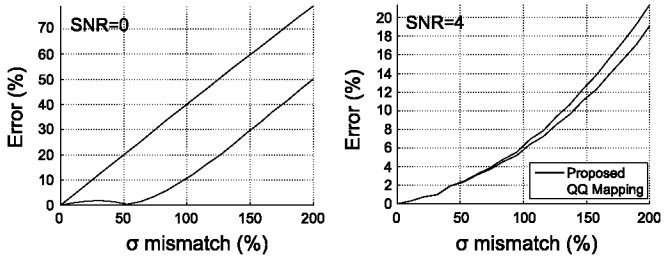

Fig. 8. Analysis of the error propagation in both the Quantile-Quantile transformation and the proposed methodology.

PD-weighted MR images (Figs. 3a, 3b, and 3c). The synthetic images were corrupted following Eq. (20). All noise patterns from Fig. 4 were used to evaluate the performance in the foreground region (the background was intentionally avoided to provide more reliable comparisons in the region of interest). The upper bounds of the noise patterns were conveniently scaled to provide a correct comparison for the SNR_{max} levels in the foreground regions. A set of 100 independent trials were used for the calculations. The spatial correlations of the noise were not considered in this experiment.

The results are depicted in Fig. 9 where it is clear that local methods (DeVore, Delakis, Maximov and Liu) give poor results in terms of averaged RE and VAR for all modalities: the RE of the methods exceeds 20 percent for $\text{SNR}_{\text{max}} > 10$. On the other hand, Goossens yields almost fixed RE and VAR parameters for $\text{SNR}_{\text{max}} > 10$ as a consequence of AWGN assumptions of the estimator, though still too high (around 20 percent). Note that the Liu's estimator is clearly outperformed by the proposed methodology, even though both Liu's and the proposed methodologies make use of the HH subband of the SWT of the image. This confirms the importance of the stabilization step in our method.

The highest accuracy among all local methods is achieved by the Landman's approach. We remind here that Maximov's and Landman's methods were initially proposed to deal with repeated acquisitions and they do not show their considerable potential in a voxelwise estimation.

The second group of the tested algorithms comprises the non-local estimators based on patch-based calculations. The leading method in this group is Manjón (2015), though it has a poorer performance for low SNR_{max} values. These results could be improved by using stacked MR data as suggested in [41], but it assumes the same underlying noise pattern in all the acquired images, which is not a realistic assumption. Borrelli's method shows a robust response for RE and VAR measures regardless of SNR_{max} level though it is always over 10 percent. Other non-local methods (Maggioni and Foi, Manjón (2010)) along with Tabelow and Pan are characterized by an extremely low VAR parameter and consequently they are preferred for image denoising procedures among non-local estimators.

Regarding the proposed method, the results show its outstanding robustness for the whole SNR range (the average RE is almost constant around 5 percent, considerably lower than any other state-of-the-art method). This behavior is of special interest when low SNR values are considered. Besides, it offers a much lower variance in the estimate, which results in a more reliable estimate.

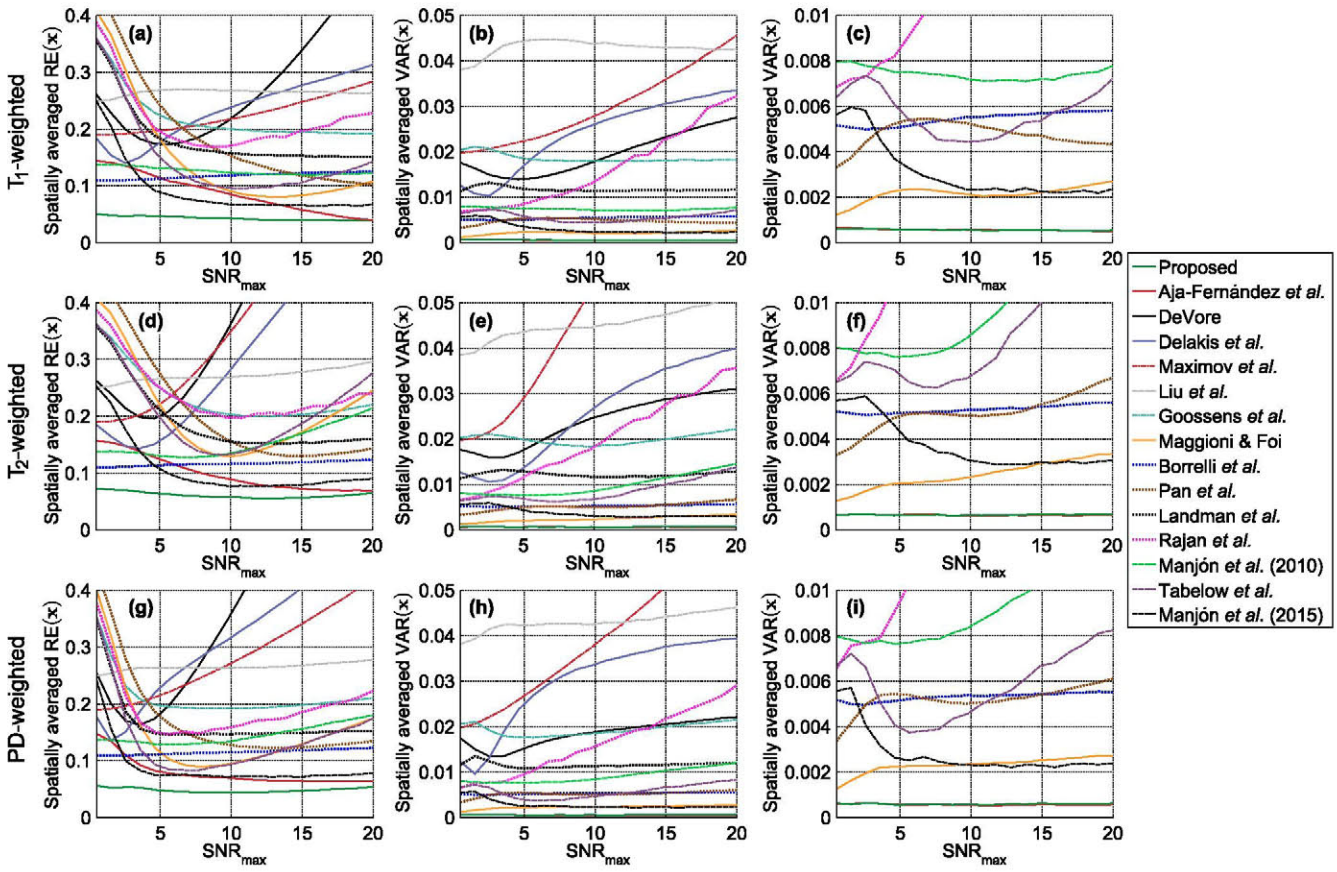

Fig. 9. Comparison of noise estimators for synthetic MR data contaminated by non-stationary Rician noise. First column: Spatially averaged relative error $\mathrm{RE}(\mathbf{x})$ of the estimators; Second column: Spatially averaged variance $\mathrm{VAR}(\mathbf{x})$ of the estimators; Third column: Zoomed $\mathrm{VAR}(\mathbf{x})$ parameter to the range $[0\text{-}0.01]$ from the second column. The first row corresponds to T_1-, the second row to T_2- and the third one to PD-weighted MRI.

We carried out a *second experiment* focused on the qualitative behavior of estimators on a synthetic T_1-weighted image contaminated by spatially variable noise following Eq. (20) and the first pattern from Fig. 4. The noise pattern is scaled to the range $[5\text{-}20]$, the exact SNR map is *a priori* known, and its maximum value equals $\mathrm{SNR}_{\max} = 8.73$. The spatial correlations of the noise component were not considered in this experiment.

The estimated noise maps and relative errors in foreground areas are shown in Fig. 10. Note that the spatial granularity shown with several techniques like DeVore, Delakis, Maximov, Liu, Goossens and Landman are due to the calculation of noise levels in fixed neighborhoods (i.e., 5×5 windows) resulting in inaccurate spatial estimations (Figs. 10a, 10b, 10c, 10d, 10e, and 10f). On the other hand, Manjón (2010), Rajan, Maggioni and Foi show a less

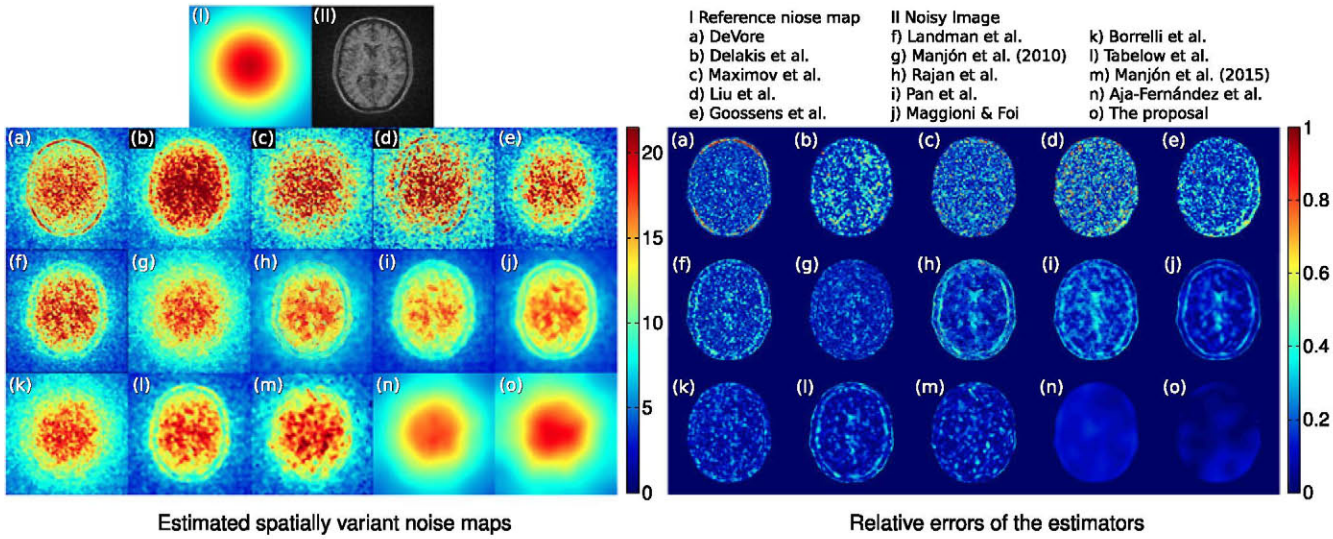

Fig. 10. Visual inspection of the methods for synthetic T_1-weighted MR brain data distorted by spatially variable noise (left figure) and corresponding relative errors of the estimators (right figure).

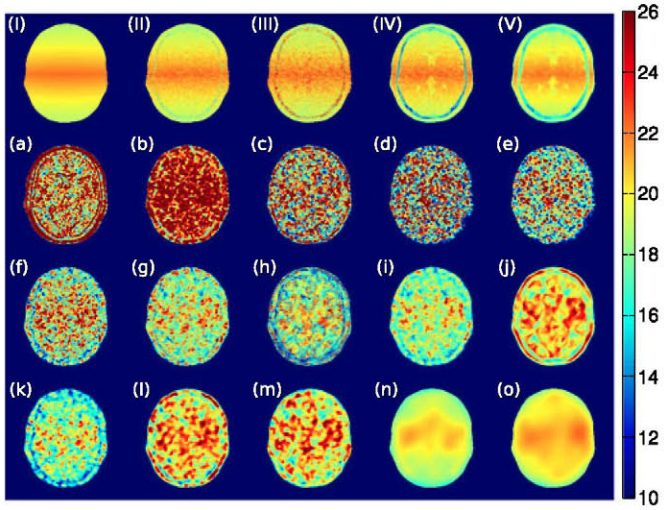

Fig. 11. Visual inspection for simulated T_1-weighted SENSE MR brain data. (I) *Ground truth* and silver standard methods for 500 repetitions: (II) DeVore, (III) Maximov, (IV) Landman and (V) Glenn (the methods follow the notation of Fig. 10).

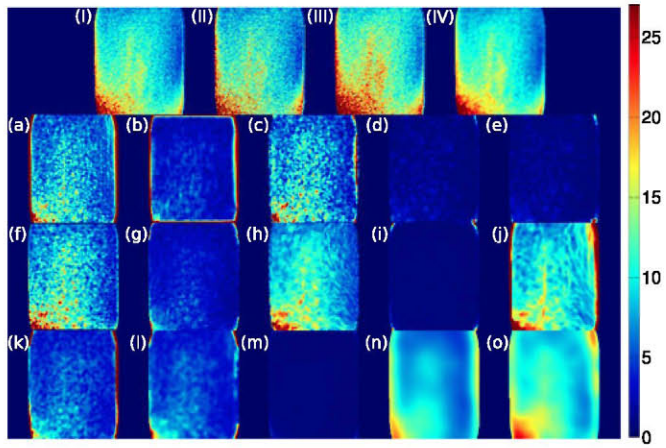

Fig. 12. Visual inspection for real T_1-weighted SENSE MRI. Silver standard methods for 20 acquisitions: (I) DeVore, (II) Maximov, (III) Landman and (IV) Glenn (the methods follow the notation of Fig. 10).

granular pattern as a result of the patch-based estimation (Figs. 10g, 10h, and 10j). A similar result was obtained from Pan's method (Fig. 10i) with the advantage of a much less computationally cost than the patch-based methods. The last advances in spatially variable noise estimation (Borrelli, Tabelow, Manjón (2015)) include an additional post-relaxation step of the raw estimates (Figs. 10k, 10l, and 10m) providing fairly smoothed and reliable noise maps, though the high-frequency components of the image (skull edges) are still observed (Fig. 10l).

Finally, Aja-Fernández and our proposal provide granular-free noise estimates without the presence of high-frequency components from the image (Figs. 10n and 10o). Some underestimation can be observed in Aja-Fernández, especially in low SNR areas, though the global pattern of the noise map is reproduced properly. In contrast, our proposal compensates these underestimations and it provides the most accurate representation of the underlying noise pattern (Fig. 10o). Moreover, our method can estimate noise levels in background regions as well, where the data follows Rayleigh distribution.

In a *third experiment*, we analyze the performance for SENSE. We considered a T_1-weighted image acquired with eight coils ($L = 8$) and subsampling rate $r = 2$ (Fig. 3d). The data coming from each coil is contaminated by AWGN with $\sigma_l^2(\mathbf{x}) = 75$ and correlation $\rho_{i,j} = 0.2$ between ith and jth coil. The image is reconstructed following the Cartesian SENSE reconstruction algorithm, which leads to a magnitude MR image affected by spatially variable, correlated and signal-dependent noise component.

Different references were considered in this experiment: the *ground truth* derivation in Aja-Fernández et al. [19] for SENSE reconstruction (Fig. 11 I) and the estimates obtained by DeVore, Maximov, Landman and Glenn methods for 500 independent replicas of the image pointwise estimated along all repetitions to provide pseudo-reference maps as *silver standard* references (Figs. 11II, 11III, 11IV, and 11V). These *silver standard* references will serve us to evaluate the methods in real images. The results shown in Figs. 11a, 11b, 11c, 11d, 11e, 11f, 11g, 11h, 11i, 11j, 11k, 11l, 11m, 11n, and 11o evidence the difficulties of estimating the spatially correlated noise. Note that local methods provide poor results and the patch-based methods do not perform better. The homomorphic approaches provide the most suitable estimates.

5.4 Real MRI Experiments

In this section we estimate the noise maps of real SENSE MRI data with two real datasets. *First*, a T_1-weighted TFE SENSE phantom reconstructed from $L = 32$ coils with subsampling rate $r = 2$ (Fig. 3e) is considered. Since the *gold standard* or *ground truth* is not available in this case, we use the aforementioned *silver standard* references (DeVore, Maximov, Landman and Glenn) obtained from the twenty acquisitions (Figs. 12I, 12II, 12III, and 12IV).

Results are depicted in Figs. 12a, 12b, 12c, 12d, 12e, 12f, 12g, 12h, 12i, 12j, 12k, 12l, 12m, 12n, and 12o, where one can see that some of the local techniques (DeVore, Maximov and Landman) perform well enough due to the local homogeneity of the source (see Figs. 12a, 12c, and 12f). The granularity of the maps comes from the small number of samples used in the estimation process (typically 5×5 windows). In comparison with the second experiment, the wavelet-based methods (Delakis, Liu, Goossens shown in Figs. 12b, 12d and 12e respectively) failed in this case. This is due to the extraction of high-frequency components using an already smooth MR image.

Maggioni and Foi's method (Fig. 12j) provides quite reasonable results, though the noise map is significantly overestimated near edges. Manjón (2010), Borrelli and Tabelow (Figs. 12g, 12k and 12l) provide highly underestimated noise patterns, but the structure of the map is still preserved. We note that Landman's and Rajan's methods (Figs. 12f and 12h) show a good behavior in the boundaries of the phantom, though the granularity is still a problem. Surprisingly, Manjón (2015) failed in this experiment, probably due to the differences in eigenvalues distribution in non-local PCA decomposition between synthetic and real MR data (Fig. 12m). Finally, Aja-Fernández (Fig. 12n) provides smooth and nongranular results but nevertheless slightly underestimated compared to the silver standards.

The proposed method (Fig. 12o) retrieves smooth and granularity-free results and it does not underestimate noise levels in foreground areas. Some overestimations can be still

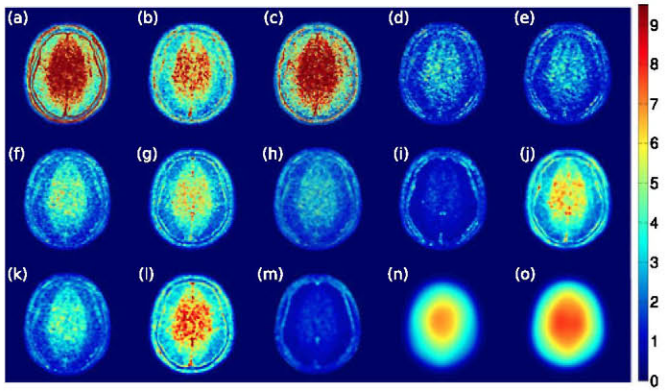

Fig. 13. Visual inspection of the methods for *in vivo* T_2-weighted FFE SENSE MRI slice from Fig. 3f. The examined methods follow the same notation as in legend as in Fig. 10.

observed near edges of the phantom. These overestimations predominantly depend on the selected noise extraction procedure (bilateral filter in this example), and could be mitigated choosing other edge-preserving and AWGN-dedicated image filtering method.

As a *second* experiment, we examine *in vivo* T_2-weighted FFE SENSE MRI brain data with subsampling rate $r = 4$ (Fig. 3f). In this case, we can only check the consistency-by visual inspection—with previous experiments due to the lack of a *ground truth* or pseudo-reference map.

Some local methods (DeVore, Delakis and Maximov) provide highly granular and overestimated noise maps especially near skull edges (Figs. 12a, 12b, and 12c). These results are consistent with the second and the third visual experiment in synthetic data. On the other hand, the methods by Liu, Goossens, Pan and Manjón (2015) show significant underestimations of the noise for *in vivo* SENSE MRI acquisition (Figs. 13d, 13e, 13i, and 13m). These results are also fully consistent with results on real phantom data shown in Fig. 12.

Maggioni/Foi and Tabelow generate consistent results with DeVore, Delakis and Maximov in the foreground area of the brain (as they did with synthetic data), although they show some overestimations in the skull edges.

Finally, the results from the method by Aja-Fernández and our proposal (Figs. 13n and 13o) are consistent with the behavior observed with synthetic data. They both provide no granular patterns, with a higher variance in the central region of the brain that was glimpsed in the other methods. No outliers are appreciated in the edges of the skull.

6 Conclusion

The spatially variable noise models have become a necessary ingredient for post-processing MR data acquired with parallel techniques. Thus, the need for suitable methods to estimate the spatially variant noise has motivated an increasing number of algorithms during the last years. In the first part of the paper, we provide an extensive analysis of the recent techniques proposed to retrieve the spatial variant noise. As we saw, most of them followed a patch-driven way to estimate the noise, leading to a granular pattern because of inaccuracies in non-homogeneous regions. The homomorphic approach of Aja-Fernández et al. [19] overcomes this limitation by assuming a high SNR, where the Gaussian assumption could hold, though it would provide important deviations in lower SNR parts of the image.

In our proposal, we suggest adopting a variance-stabilization strategy to transform the signal-dependence of noise into a signal independent noise map. To do so, we propose a parametric version of the formulation of the asymptotic Rician stabilizer proposed by Foi [49] whose parameters are efficiently estimated for different SNRs. In order to provide a Gaussian-like behavior of the transformed noise, we impose constraints on the kurtosis and skewness as well as Gaussian-like resulting distribution. The transformation was tested for both low SNRs and asymptotic SNRs showing an outstanding behavior in the whole range. Additionally, the statistical tests confirm the Gaussian-like behavior of noise which results in an efficient extraction of noise performed by a homomorphic transformation, which avoids the granular effect of pixelwise and patch-driven methods. The unbiased estimation under the Gaussian assumption can be efficiently calculated due to the results of [14].

The limitations of our method are the need of an initial $\widehat{\sigma_0(\mathbf{x})}$ and the SNR. However, the method has proven to be robust to this initialization showing important improvements when initialized with the state-of-the-art methods. This fact was confirmed when the worst case obtained with the proposed method was compared to the best case of the methods of literature, showing its suitability and robustness.

The performance of our method in synthetic and real images show that both the stabilization process and the homomorphic estimation eliminate the granularity, reduce the under/overestimation of noise and lead to more reliable estimates (low relative error and very low spatial variance).

The main contributions of the proposed method, when compared to the state of the art, are: 1) It does not depend on repeated acquisitions and/or a biophysical model of the data. 2) Any additional information like sensitivity profiles or noise matrices in the receiver coils is also unnecessary. 3) Just one single image without background or foreground region extraction is required. 4) The method works for different MR modalities: T_1-weighted, T_2-weighted and PD-weighted MR data. 5) It is not affected by granular effect due to local estimation. 6) It works for the whole range of SNRs from the very low to the asymptotically Gaussian.

Our estimation methodology serves as an initial phase of further MR image processing pipeline as could be image denoising in the MRI field requiring an estimate of the variant noise. Additionally, note that although the proposed VST homomorphic filter is designed for non-stationary Rician noise, it can be easily extended to other distributions presented in MRI, like the non-stationary nc-χ.

Acknowledgments

The authors thank M. Maggioni and K. Tabelow for sharing the source codes of their methods and for their outstanding assistance. This work was supported by Ministerio de Ciencia e Innovación with research grant TEC2013-44194-P. T. Pieciak acknowledges National Science Centre, Poland, for funding resource (2015/19/N/ST7/01204). Gonzalo Vegas-Sánchez-Ferrero acknowledges Consejería de Educación, Juventud y Deporte of Comunidad de Madrid and the People Programme (Marie Curie Actions)

of the European Unions Seventh Framework Programme (FP7/2007-2013) for REA grant agreement n. 291820.

REFERENCES

[1] G. K. Rohde, A. S. Barnett, P. J. Basser, and C. Pierpaoli, "Estimating intensity variance due to noise in registered images: Applications to diffusion tensor MRI," *NeuroImage*, vol. 26, no. 3, pp. 673–684, 2005.

[2] J. K. Gahm, G. Kindlmann, and D. B. Ennis, "The effects of noise over the complete space of diffusion tensor shape," *Med. Image Anal.*, vol. 18, no. 1, pp. 197–210, 2014.

[3] A. Reichenbach, M. Hlawitschka, M. Tittgemeyer, and G. Scheuermann, "Choosing a tractography algorithm: On the effects of measurement noise," in *Computational Diffusion MRI and Brain Connectivity*. Berlin, Germany: Springer, 2014, pp. 115–128.

[4] J. Noh and V. Solo, "Rician distributed fMRI: Asymptotic power analysis and Cramer-Rao lower bounds," *IEEE Trans. Signal Process.*, vol. 59, no. 3, pp. 1322–1328, Mar. 2011.

[5] N. Dikaios, et al., "Noise estimation from averaged diffusion weighted images: Can unbiased quantitative decay parameters assist cancer evaluation?" *Magn. Resonance Med.*, vol. 71, no. 6, pp. 2105–2117, 2014.

[6] A. den Dekker and J. Sijbers, "Data distributions in magnetic resonance images: A review," *Phys. Medica*, vol. 30, no. 7, pp. 725–741, 2014.

[7] M. Henkelman, "Measurement of signal intensities in the presence of noise in MR images," *Med. Phys.*, vol. 12, pp. 232–233, 1985.

[8] H. Gudbjartsson and S. Patz, "The Rician distribution of noisy MRI data," *Magn. Resonance Med.*, vol. 34, no. 6, pp. 910–914, 1995.

[9] D. O. Walsh, A. F. Gmitro, and M. W. Marcellin, "Adaptive reconstruction of phased array MR imagery," *Magn. Resonance Med.*, vol. 43, no. 5, pp. 682–690, 2000.

[10] C. Constantinides, E. Atalar, and E. McVeigh, "Signal-to-noise measurements in magnitude images from NMR phased arrays," *Magn. Resonance Med.*, vol. 38, no. 5, pp. 852–857, 1997.

[11] S. Aja-Fernández and A. Tristán-Vega, "Influence of noise correlation in multiple-coil statistical models with sum of squares reconstruction," *Magn. Resonance Med.*, vol. 67, pp. 580–585, 2012.

[12] K. P. Pruessmann, M. Weiger, M. B. Scheidegger, and P. Boesiger, "SENSE: Sensitivity encoding for fast MRI," *Magn. Resonance Med.*, vol. 42, no. 5, pp. 952–962, 1999.

[13] M. A. Griswold, et al., "Generalized autocalibrating partially parallel acquisitions (GRAPPA)," *Magn. Resonance Med.*, vol. 47, no. 6, pp. 1202–1210, 2002.

[14] S. Aja-Fernández, T. Pieciak, and G. Vegas-Sánchez-Ferrero, "Spatially variant noise estimation in MRI: A homomorphic approach," *Med. Imag. Anal.*, vol. 20, no. 1, pp. 184–197, 2015.

[15] S. Aja-Fernández, A. Tristán-Vega, and W. Hoge, "Statistical noise analysis in GRAPPA using a parametrized noncentral Chi approximation model," *Magn. Resonance Med.*, vol. 65, pp. 1195–1206, 2011.

[16] S. Aja-Fernández, A. Tristán-Vega, and C. Alberola-López, "Noise estimation in single-and multiple-coil magnetic resonance data based on statistical models," *Magn. Resonance Imag.*, vol. 27, no. 10, pp. 1397–1409, 2009.

[17] J. Sijbers, D. Poot, A. den Dekker, and W. Pintjens, "Automatic estimation of the noise variance from the histogram of a magnetic resonance image," *Phys. Med. Biol.*, vol. 52, pp. 1335–1348, 2007.

[18] A. A. Samsonov and C. R. Johnson, "Noise-adaptive nonlinear diffusion filtering of MR images with spatially varying noise levels," *Magn. Resonance Med.*, vol. 52, no. 4, pp. 798–806, 2004.

[19] S. Aja-Fernández, G. Vegas-Sánchez-Ferrero, and A. Tristán-Vega, "Noise estimation in parallel MRI: GRAPPA and SENSE," *Magn. Resonance Imag.*, vol. 32, no. 3, pp. 281–290, 2014.

[20] B. A. Landman, P.-L. Bazin, S. A. Smith, and J. L. Prince, "Robust estimation of spatially variable noise fields," *Magn. Resonance Med.*, vol. 62, no. 2, pp. 500–509, 2009.

[21] I. I. Maximov, E. Farrher, F. Grinberg, and N. Jon Shah, "Spatially variable Rician noise in magnetic resonance imaging," *Med. Image Anal.*, vol. 16, no. 2, pp. 536–548, 2012.

[22] J. Veraart, J. Rajan, R. R. Peeters, A. Leemans, S. Sunaert, and J. Sijbers, "Comprehensive framework for accurate diffusion MRI parameter estimation," *Magn. Resonance Med.*, vol. 70, no. 4, pp. 972–984, 2013.

[23] G. R. Glenn, A. Tabesh, and J. H. Jensen, "A simple noise correction scheme for diffusional kurtosis imaging," *Magn. Resonance Imag.*, vol. 33, no. 1, pp. 124–133, 2015.

[24] T. L. Marzetta, "EM algorithm for estimating the parameters of a multivariate complex Rician density for polarimetric SAR," in *Proc. IEEE Int. Conf. Acoust. Speech Signal Process.*, 1995, vol. 5, pp. 3651–3654.

[25] M. D. DeVore, A. D. Lanterman, and J. A. O'Sullivan, "ATR performance of a Rician model for SAR images," in *Proc. SPIE Automat. Target Recognit.*, 2000, pp. 34–45.

[26] B. Goossens, A. Pizurica, and W. Philips, "Wavelet domain image denoising for non-stationary noise and signal-dependent noise," in *Proc. IEEE Int. Conf. Image Process.*, 2006, pp. 1425–1428.

[27] I. Delakis, O. Hammad, and R. I. Kitney, "Wavelet-based de-noising algorithm for images acquired with parallel magnetic resonance imaging (MRI)," *Phys. Med. Biol.*, vol. 52, 2007, Art. no. 3741.

[28] B. A. Landman, P.-L. Bazin, and J. L. Prince, "Estimation and application of spatially variable noise fields in diffusion tensor imaging," *Magn. Resonance Imag.*, vol. 27, no. 6, pp. 741–751, 2009.

[29] W. Guo and F. Huang, "Adaptive Total Variation based filtering for MRI images with spatially inhomogeneous noise and artifacts," in *Proc. 6th IEEE Int. Symp. Biomed. Imag.*, 2009, pp. 101–104.

[30] Y. Ding, Y.-C. Chung, and O. P. Simonetti, "A method to assess spatially variant noise in dynamic MR image series," *Magn. Resonance Med.*, vol. 63, no. 3, pp. 782–789, 2010.

[31] J. V. Manjón, P. Coupé, L. Martí-Bonmatí, D. L. Collins, and M. Robles, "Adaptive non-local means denoising of MR images with spatially varying noise levels," *J. Magn. Resonance Imag.*, vol. 31, no. 1, pp. 192–203, 2010.

[32] J. Rajan, D. Poot, J. Juntu, and J. Sijbers, "Maximum likelihood estimation-based denoising of magnetic resonance images using restricted local neighborhoods," *Phys. Med. Biol.*, vol. 56, no. 16, pp. 5221–5234, 2011.

[33] M. Maggioni and A. Foi, "Nonlocal transform-domain denoising of volumetric data with groupwise adaptive variance estimation," in *Proc. IS&T/SPIE Electron. Imag.*, 2012, pp. 82960O–82960O.

[34] X. Pan, X. Zhang, and S. Lyu, "Blind local noise estimation for medical images reconstructed from rapid acquisition," in *Proc. SPIE Med. Imag.*, 2012, pp. 83143R–83143R.

[35] S. Aja-Fernández, V. Brion, and A. Tristán-Vega, "Effective noise estimation and filtering from correlated multiple-coil MR data," *Magn. Resonance Imag.*, vol. 31, no. 2, pp. 272–285, 2013.

[36] R. W. Liu, L. Shi, W. Huang, J. Xu, S. C. H. Yu, and D. Wang, "Generalized total variation-based MRI Rician denoising model with spatially adaptive regularization parameters," *Magn. Resonance Imag.*, vol. 32, no. 6, pp. 702–720, 2014.

[37] P. Borrelli, G. Palma, M. Comerci, and B. Alfano, "Unbiased noise estimation and denoising in parallel magnetic resonance imaging," in *Proc. IEEE Int. Conf. Acoust. Speech Signal Process.*, 2014, pp. 1230–1234.

[38] M. S. Hansen, S. J. Inati, and P. Kellman, "Noise propagation in region of interest measurements," *Magn. Resonance Med.*, vol. 73, no. 3, pp. 1300–1308, 2015.

[39] K. Tabelow, H. U. Voss, and J. Polzehl, "Local estimation of the noise level in MRI using structural adaptation," *Med. Image Anal.*, vol. 20, no. 1, pp. 76–86, 2015.

[40] S. Aja-Fernández and G. Vegas-Sánchez-Ferrero, "Blind estimation of spatially variant noise in GRAPPA MRI," in *Proc. IEEE Int. Symp. Biomed. Imag.*, 2015, pp. 1478–1481.

[41] J. V. Manjón, P. Coupé, and A. Buades, "MRI noise estimation and denoising using non-local PCA," *Med. Image Anal.*, vol. 22, no. 1, pp. 35–47, 2015.

[42] D. Poot and S. Klein, "Detecting statistically significant differences in quantitative MRI experiments, applied to diffusion tensor imaging," *IEEE Trans. Med. Imag.*, vol. 34, no. 5, pp. 1164–1176, May 2015.

[43] J. Veraart, E. Fieremans, and D. S. Novikov, "Diffusion MRI noise mapping using random matrix theory," *Magn. Resonance Med.*, vol. 76, pp. 1582–1593, 2016.

[44] J. Sijbers, A. den Dekker, J. V. Audekerke, M. Verhoye, and D. V. Dyck, "Estimation of the noise in magnitude MR images," *Magn. Resonance Imag.*, vol. 16, no. 1, pp. 87–90, 1998.

[45] C. G. Koay and P. J. Basser, "Analytically exact correction scheme for signal extraction from noisy magnitude MR signals," *J. Magn. Resonance*, vol. 179, no. 2, pp. 317–322, 2006.

[46] P. Coupé, J. V. Manjón, E. Gedamu, D. Arnold, M. Robles, and D. L. Collins, "Robust Rician noise estimation for MR images," *Med. Image Anal.*, vol. 14, no. 4, pp. 483–493, 2010.
[47] M. S. Bartlett, "The use of transformations," *Biometrics*, vol. 3, no. 1, pp. 39–52, 1947.
[48] P. Billingsley, *Probability and Measure*, 3rd ed. Hoboken, NJ, USA: Wiley, Apr. 1995.
[49] A. Foi, "Noise estimation and removal in MR imaging: The variance-stabilization approach," in *Proc. IEEE Int. Symp. Biomed. Imag.*, 2011, pp. 1809–1814.
[50] M. Maggioni, V. Katkovnik, K. Egiazarian, and A. Foi, "Nonlocal transform-domain filter for volumetric data denoising and reconstruction," *IEEE Trans. Image Process.*, vol. 22, no. 1, pp. 119–133, Jan. 2013.
[51] C. G. Koay, E. Özarslan, and P. J. Basser, "A signal transformational framework for breaking the noise floor and its applications in MRI," *J. Magn. Resonance Imag.*, vol. 197, no. 2, pp. 108–119, 2009.
[52] M. Makitalo and A. Foi, "Optimal inversion of the Anscombe transformation in low-count Poisson image denoising," *IEEE Trans. Image Process.*, vol. 20, no. 1, pp. 99–109, Jan. 2011.
[53] C. Tomasi and R. Manduchi, "Bilateral filtering for gray and color images," in *Proc. 6th Int. Conf. Comput. Vis.*, 1998, pp. 839–846.
[54] D. Collins, et al., "Design and construction of a realistic digital brain phantom," *IEEE Trans. Med. Imag.*, vol. 17, no. 3, pp. 463–468, Jun. 1998.